

Patterns of energy-dependent variability from Comptonization

Marek Gierliński^{1,2*} and Andrzej A. Zdziarski³

¹*Department of Physics, University of Durham, South Road, Durham DH1 3LE, UK*

²*Astronomical Observatory, Jagiellonian University, Orla 171, 30-244 Kraków, Poland*

³*Centrum Astronomiczne im. M. Kopernika, Bartycza 18, 00-716 Warszawa, Poland*

Submitted to MNRAS

ABSTRACT

We study fractional variability as a function of energy from black-hole X-ray binaries on timescales from milliseconds to hundreds of seconds. We build a theoretical model of energy-dependent variability in which the X-ray energy spectrum varies in response to a changing physical parameter. We compare these models to rms spectra obtained from *RXTE* PCA observations of black-hole binaries XTE J1550–564 and XTE J1650–500. We show that two main variability models are consistent with the data: variable seed photon input in the hard state and variable power in the Comptonized component in the soft and very high states. The lack of clear reflection features in the rms spectra implies that the reflection and the X-ray continuum, when integrated over Fourier frequencies, are correlated and vary with similar fractional amplitudes. Our models predict two important features of rms spectra, not possible to be clearly seen by the PCA due sensitivity limits. At soft X-rays, $\lesssim 3$ keV, we predict the presence of a break in the rms spectrum at energy directly related to the seed photon temperature. At higher energies, ~ 20 – 30 keV, we predict a peak in the rms spectrum originating from the variability of the spectrum produced by a hybrid thermal/non-thermal electron distribution. If these features are confirmed by broad-band observations, they will impose important constraints on the origin of the seed photons for Comptonization and the electron distribution in the hot plasma.

Key words: accretion, accretion discs – radiation mechanisms: non-thermal – stars: individual: XTE J1550–564 – stars: individual: XTE J1650–500 – X-rays: binaries.

1 INTRODUCTION

X-ray emission from accreting black holes is commonly thought to originate from inverse Compton scattering of cooler disc photons in a hot optically thin plasma. Depending on the geometry of the accretion flow and the distribution of power between the disc and the hot plasma, a variety of spectral distributions can be produced. This translates into a variety of observed spectral states. One approach to understanding the physics of accretion is by fitting various models to the time-averaged energy spectra. The spectral decomposition of the data is fairly well understood, and typically requires a model consisting of disc emission, its Comptonization and Compton reflection of the hard X-ray photons from the disc (see e.g. Zdziarski & Gierliński 2004 and references therein).

Another approach to the X-ray data is by analysing their variability on various timescales. Fast aperiodic variability on the timescales from milliseconds to hundreds of seconds is often studied using power density spectra (PDS), in particular, by tracing quasi-periodic oscillations (QPO). For a review, see van der Klis (2004). Most of this variability occurs on dynamical timescales in the inner part of the accretion flow, so it makes an excellent

probe of the deep gravitational potential around the compact object. However, despite huge amounts of available data, we are still far from understanding of *how* the rapid X-ray variability is produced. Many of existing models propose oscillations in the accretion disc (e.g. Cui, Zhang & Chen 1998; Titarchuk, Osherovich & Kuznetsov 1999; Psaltis & Norman 2000) as the origin of variability. Though these models have been successful in explaining observed characteristic frequencies, it is not clear how oscillations of the disc are translated into varying X-rays. Giannios & Spruit (2004) proposed that QPOs in the inner hot flow can be excited by interaction between the flow and the outer cold disc (e.g. by cooling-heating feedback loop). Bursa et al. (2004) suggested that hard X-rays can be modulated via gravitational lensing of the oscillating accretion flow in the vicinity of the black hole. Another suggestion involves dense cold blobs of material drifting through the inhomogeneous hot inner flow and providing with a variable source of the seed photons for Comptonization (Böttcher & Liang 1999). An alternative set of models that can directly explain the origin of X-ray modulation invokes propagation of X-ray flares in the accretion flow (e.g. Böttcher & Liang 1998; Poutanen & Fabian 1999; Zych 2003).

There are a few possibilities of bridging over the fairly well understood energy spectra and the enigmatic variability. One of

* E-mail: Marek.Gierlinski@durham.ac.uk

them is to study how X-ray energy spectra change with the Fourier frequency, by means of the so-called frequency-resolved spectroscopy. A handful of bright objects have been studied this way, both containing black holes (Revnivtsev, Gilfanov & Churazov 1999b, 2001) and neutron stars (Gilfanov, Revnivtsev & Molkov 2003). A number of important conclusions have been obtained from these data. One particularly interesting result is that the strength of Compton reflection in the low/hard state of black-hole binaries significantly decreases with the increasing Fourier frequency.

Another promising but not yet very well studied field of research is the energy dependence of rapid X-ray variability. It can bridge over the fairly well understood energy spectra and the enigmatic variability. The simplest approach is by looking at the fractional root mean square variability amplitude (integrated over a range of frequencies or timescales) as a function of energy, $\text{rms}(E)$, or in other words, a relative variability spectrum. Such a spectrum can tell us about how the spectral components (disc or Comptonization) vary with respect to each other and whether they change their spectral shape on the observed timescales. Variability spectra have been recently obtained both from Galactic and supermassive black holes (e.g. Revnivtsev, Borozdin & Emelyanov 1999a; Lin et al. 2000; Wardziński et al. 2002; Vaughan & Fabian 2004). Also, the amplitude of QPOs as a function of energy has also been studied (e.g. Rao et al. 2000; Gilfanov et al. 2003; Rodriguez et al. 2004a, b). However, until recently, little theoretical interpretation was given. Zdziarski (2005) proposed a theoretical model considering radial dependence of the local variability in the disc. By assuming the local rms and disc temperature decreasing with increasing radius, he found an $\text{rms}(E)$ increasing with energy, consistent, e.g., with an ultrasoft state of GRS 1915+105. Zdziarski et al. (2002), hereafter Z02, analysed the spectral variability of Cyg X-1 from the *RXTE*/ASM and *CGRO*/BATSE on timescales of days and months, and reported two distinct patterns of $\text{rms}(E)$ in different spectral states. They proposed that in the hard state the variability was driven by changes in the inner radius of the truncated disc, which in turn varied the seed photon input for Comptonization. In the soft state, it was brought about by variations of the power released in a hot corona above the disc.

In this paper, we investigate patterns of $\text{rms}(E)$ variability generated by variations of physical properties of the accretion flow. We consider a particular spectral model of a hybrid, thermal/non-thermal Comptonization and study the effects of varying parameters of this model. We compare the results with rms spectra of rapid X-ray variability of two Galactic black holes, XTE J1650–500 and XTE J1550–564.

We would like to point out that our variability spectra have their own limitations. First, we have chosen to integrate them over a wide range of Fourier frequencies (those available to the *RXTE*/PCA instrument, see Section 2 below), while the spectral dependence on frequency has been shown to be important in some cases, see, e.g., Revnivtsev et al. (1999b). We note that it is entirely possible to create $\text{rms}(E)$ integrated over a narrow range of frequencies, and then that $\text{rms}(E)$ times the average spectrum will be equal to the corresponding frequency-resolved spectrum. Such an analysis is, however, beyond the scope of the present work because it would increase the dimension of the parameter space, thus leading to a substantial increase of the complexity of the study. Also, that approach requires data of significantly higher statistics than those required in the case of integration over all available frequencies. Consequently, the results on interpretation of X-ray data presented here are mostly valid for the range of frequencies dominating the power spectrum (typically ~ 0.1 –10 Hz, see Section 5 be-

low). On the other hand, our theoretical results are general, and can be directly applied to frequency-resolved $\text{rms}(E)$ in future work.

Furthermore, neither $\text{rms}(E)$ nor frequency-resolved spectra carry information about either phase/time lags (for a review see Poutanen 2001 and references therein) or coherence (Vaughan & Nowak 1997) between signals at different energies at a given Fourier frequency. Also, our theoretical interpretation of $\text{rms}(E)$ is based on a one-component model of Comptonization. Thus, this approach does not deal with, e.g., propagation effects, likely to be important in actual flows (e.g. Kotov, Churazov & Gilfanov 2001).

2 DATA REDUCTION

We have analysed several observations (with unique identifiers, called obsids) of XTE J1650–500 and XTE J1550–564 from the *RXTE* PCA and HEXTE detectors. For data reduction, we used *FTOOLS* 5.3. We extracted energy spectra from the top layer of the detector 2 of the PCA and added a 1 per cent systematic error in each channel. We extracted HEXTE spectra from both clusters. For energy spectra, we use the PCA data in 3–20 keV band and the HEXTE data in 20–200 keV band.

We extracted rms spectra from the PCA data using the following approach (see also Zdziarski et al. 2005). First, we extracted light curves with 1/256-s resolution for the PCA absolute energy channels 0–71 (corresponding to energies from ~ 2 to about 25–30 keV, depending on the PCA epoch). Some of the channels were binned together to improve statistics. Then, we calculated PDS from each of the light curves (over 512-s intervals), subtracted the Poissonian noise, corrected for dead-time effects (Revnivtsev, Gilfanov & Churazov 2000) and background (Berger & van der Klis 1994). The energy-dependent rms was found by integrating the PDS over the (1/512)–128 Hz frequency band.

We would like to stress the importance of background correction of the power spectra. The fractional rms we use in this paper is the standard deviation divided by the mean source count rate, which obviously must exclude the background count rate (see also Berger & van der Klis 1994). The background variability is assumed to be Poissonian and is subtracted from the PDS. At higher energies, $\gtrsim 30$ keV, estimating the PCA background, which dominates most of the spectra, becomes less reliable, so does the calculated rms. We discuss possible effects of the high-energy background estimation in Section 5.3.

3 THE METHOD

Fractional variability spectra are the result of the observed flux varying differently at different energies. In order to devise any theoretical model of energy-dependent variability, one has to make certain assumptions about the energy spectrum. We do so by fitting the observed spectra by a physically motivated model.

3.1 The Comptonization model

In this paper, we use a spectral model consisting of a soft component, modelled by the multicolour blackbody disc emission (Mitsuda et al. 1984), Comptonization of seed photons in the hybrid plasma (EQPAIR), and reflection of the Comptonized photons from the cold disc (Magdziarz & Zdziarski 1995). The model EQPAIR (Coppi 1999; Gierliński et al. 1999) calculates self-consistently microscopic processes in a hot plasma with electron acceleration at a

power-law rate with an index Γ_{inj} , in a background thermal plasma with a Thomson optical depth of ionization electrons, τ . The electron temperature, T , is calculated from the balance of Compton and Coulomb energy exchange, taking into account pair production as well. The last two processes depend on the plasma compactness, $\ell \equiv \mathcal{L}\sigma_{\text{T}}/(\mathcal{R}m_e c^3)$, where \mathcal{L} is a power supplied to the hot plasma, \mathcal{R} is its characteristic size, and σ_{T} is the Thomson cross section. We then define the hard compactness, ℓ_{h} , corresponding to the power supplied to the electrons, and the soft compactness, ℓ_{s} , corresponding to the power in soft seed photons irradiating the plasma (which are assumed to be emitted by a blackbody disk with the maximum temperature, T_{s}). The compactness corresponding to the electron acceleration and to a direct heating of the thermal electrons are denoted as ℓ_{nth} and ℓ_{th} , respectively, and $\ell_{\text{h}} = \ell_{\text{nth}} + \ell_{\text{th}}$. Details of the model are given in Gierliński et al. (1999). The non-thermal electrons are accelerated between the Lorentz factors γ_{min} and γ_{max} , which we assume to be 1.3 and 100, respectively.

We then use the best-fitting spectral model to build $\text{rms}(E)$ models which we can compare with variability data. Here we apply two different approaches to $\text{rms}(E)$ spectra: a simple ‘two-component’ model that has been used in previous works, and a novel variable parameter idea, based on physics of emission of the accretion flow.

3.2 Two-component variability

The simplest approach to energy-dependent variability is to consider a number of spectral components with different variability amplitudes. We assume in this paper that the energy spectrum consists of two components, the soft (blackbody disc) and the hard (Comptonization). We neglect reflection variability in this model, but discuss its possible effects in Section 7. When the spectral components vary with different variances they create energy-dependent variability, as fraction of each component in the total spectrum changes as a function of energy. The total variance at a given energy, E , is

$$\sigma^2(E) = \sigma_{\text{s}}^2(E) + \sigma_{\text{h}}^2(E) + 2\sigma_{\text{sh}}(E), \quad (1)$$

where $\sigma_{\text{s}}^2(E)$ and $\sigma_{\text{h}}^2(E)$ are the soft and hard variances and $\sigma_{\text{sh}}(E)$ is their covariance. In the following approach, we assume that the soft and hard component variabilities are fully correlated, so $\sigma_{\text{sh}}(E) = \sigma_{\text{s}}(E)\sigma_{\text{h}}(E)$ and thus

$$\sigma(E) = \sigma_{\text{s}}(E) + \sigma_{\text{h}}(E). \quad (2)$$

We define fractional rms variability as $\text{rms}(E) \equiv \sigma(E)/F(E)$, where $F(E)$ is the time-averaged flux. The total fractional rms variability is

$$\text{rms}(E) = r(N_{\text{s}}) \frac{F_{\text{s}}(E)}{F(E)} + r(N_{\text{h}}) \frac{F_{\text{h}}(E)}{F(E)}. \quad (3)$$

The $F(E)$, $F_{\text{s}}(E)$ and $F_{\text{h}}(E)$ are taken from the best-fitting spectral models, while $r(N_{\text{s}})$ and $r(N_{\text{h}})$ are free parameters. As fractional variabilities of the normalization, $r(N_{\text{s}})$ and $r(N_{\text{h}})$ are energy-independent quantities.

The two- or multicomponent approach has been used for variability studies before (e.g., Rao et al. 2000; Vaughan & Fabian 2004; Zdziarski et al. 2005). There are, however, obvious caveats of this model, as it does not take spectral variability of Comptonization into account. Clearly, where the physical properties of the accretion flow change, we expect, in particular, the spectral slope of Comptonization to vary as well.

3.3 Parameter variability

Therefore, we have created another model based on variability of physical properties of the accretion flow. Our spectral model (Section 3.1, consisting of the multicolour blackbody disc and Comptonization (again, we neglect effects of reflection on variability), is a function of several parameters: $F = F(p_1, p_2, \dots, p_n, E)$. We allow for variation of a given parameter p_i with Gaussian distribution (but we test lognormal distribution as well) around its best-fitting mean value \bar{p}_i with standard deviation $\sigma(p_i)$ [or fractional rms $r(p_i) \equiv \sigma(p_i)/\bar{p}_i$]. This, in turn, causes the whole X-ray spectrum to vary, generating various patterns of energy-dependent variability. Below, we concentrate on varying soft (ℓ_{s}) and hard (ℓ_{h}) compactness of Comptonization, which correspond to varying luminosity or power released in the seed photons and electrons, respectively. We also check for effects of other parameters varying.

4 RESULTS

4.1 Hard state

Fig. 1(a) shows an rms spectrum of the black hole binary XTE J1650–500 in the hard X-ray spectral state. This type of spectrum, where fractional rms variability decreases with energy is common in the hard state of black hole binaries. Another common variability type in this state is a flat $\text{rms}(E)$, which we discuss later in the paper. We are going to interpret the observed $\text{rms}(E)$ making use of the energy spectral model fitted to the PCA/HEXTE data. The energy spectrum of this observation with its best-fitting model is presented in Fig. 1(b). It is well described ($\chi^2_{\nu} = 132/129$) by purely thermal Comptonization in a plasma with the hard-to-soft compactness ratio of $\ell_{\text{h}}/\ell_{\text{s}} = 3.8^{+0.2}_{-0.1}$, and the optical depth, $\tau = 1.82^{+0.13}_{-0.06}$. The self-consistently computed temperature of the electrons is 47 keV, and the soft component temperature is $kT_{\text{s}} = 0.72^{+0.25}_{-0.19}$ keV. We also found Compton reflection with the amplitude of $\Omega/2\pi = 0.18 \pm 0.03$ and the ionization of the reflector of $\lg(\xi/1 \text{ erg cm s}^{-1}) = 3.1 \pm 0.2$. This kind of a spectrum is typical of black-hole binaries (e.g. Gierliński et al. 1997; Zdziarski et al. 1998; Di Salvo et al. 2001) in the hard state (but see our discussion of the soft component in Section 5.1).

We first try the two-component model, considering soft and Comptonized components varying in luminosity, but not in the spectral shape. When the energy spectrum is dominated by one component, the amplitude of variability does not depend on energy. A spectrum varying in normalization only yields the same *fractional* variability amplitude at all energies, regardless of its spectral shape. Therefore, at energies $\gtrsim 5$ keV, where Comptonization dominates, the predicted rms spectrum is flat. This behaviour is not consistent with the observed $\text{rms}(E)$ relation in the hard state of XTE J1650–500, where the rms amplitude decreases with energy. In Fig. 1(a) we show a model of two-component variability pattern (dashed curve) compared to the data. Clearly, this kind of variability is not consistent with observations. Including reflection as a third independently varying component cannot resolve this problem either.

Then, to explain the decreasing $\text{rms}(E)$ in the hard state, we considered variability of the seed photon input (Z02). We allowed for variations in the soft component normalization, N_{s} (but not in its temperature). We assumed that the seed photons for Comptonization originated from the soft spectral component. Therefore, ℓ_{s} was linearly proportional to the soft component luminosity, so it varied with the same fractional rms as N_{s} . The hard compact-

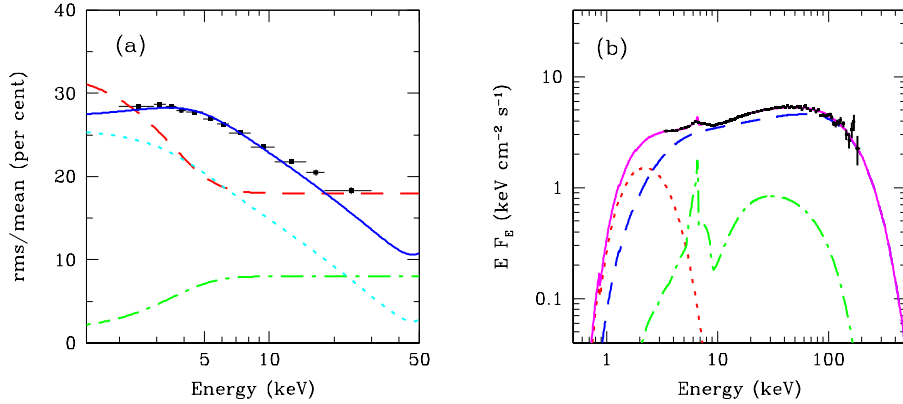


Figure 1. (a) Hard state (obsid 60113-01-04-00) rms spectrum of XTE J1650–500 observed by *RXTE*. The dashed curve (red in colour) represents the two-component variability model, with $r(N_s) = 36\%$ and $r(N_h) = 18\%$, clearly not consistent with the data. The solid (blue in colour) curve shows the model with varying soft photon input (dotted curve, cyan in colour) at $r(\ell_s) = 25\%$ plus an additional hard component normalization variability (dash-dotted curve, green in colour) with $r(N_h) = 8\%$. (b) Energy spectrum of the same observation, with the unfolded PCA and HEXTE data together with the best-fitting model. The model consists of the following components: the soft component modelled by DISKBB (dotted curve, red in colour, showing unscattered seed photons only), its Comptonization in thermal plasma (dashed curve, blue in colour), and reflection (dash-dotted curve, green in colour). The solid curve (magenta in colour) shows their sum.

ness, ℓ_h , was constant, so the hard-to-soft compactness ratio, ℓ_h/ℓ_s , varied as well. The hard-to-soft compactness ratio sets the energy balance between the seed photons and hot electrons, and is directly responsible for the hardness (spectral index) of the energy spectrum (e.g., Coppi 1999). Therefore, varying ℓ_s caused pivoting of the whole spectrum around ~ 50 keV (as shown in Fig. 4a). We assumed $\bar{\ell}_s = 10$ and $r(\ell_s) = 25\%$. As a result, the fractional rms decreased with energy, as showed by the dotted (cyan in colour) curve in Fig. 1(a). This model was well below the observed rms, but simply increasing ℓ_s variability did not help because at a higher $r(\ell_s)$ the model rms(E) became much steeper than the observed one. To resolve the problem we allowed for additional variability of the hard component luminosity (or normalization), with $r(N_h) = 8\%$. The resulting rms(E) matched the data well. We note that we have not performed formal fits of our models to the observed rms spectra. We have only found a model that visually matched the observed rms pattern. This best-matching model can be interpreted as strongly varying seed photon input (resulting in the pivoting hard component) accompanied by a much weaker variation in the hard component luminosity. We have tested other model parameters variability, but none of them produced rms(E) even remotely consistent with the data.

We also tested the effect of a probability distribution of varying ℓ_s different than Gaussian. A feasible alternative is to use lognormal distribution, as it has been found to fit the distribution of fluxes from Cyg X-1 (Uttley, McHardy & Vaughan 2005). We have repeated the above calculations for a lognormal distribution of ℓ_s and found only negligible difference between the lognormal and Gaussian distribution results.

4.2 Soft state

Fig. 2(a) shows an rms spectrum of XTE J1650–500 in the soft X-ray spectral state. The pattern of variability is distinctly different from the hard state in Fig. 1(a). It rises with energy and saturates above ~ 10 keV. We have looked through all rms spectra of XTE J1650–500 and found that this pattern is characteristic for all the soft state spectra.

The soft-state energy spectrum (Fig. 2b) is well described ($\chi^2_\nu = 115/117$) by a hybrid Comptonization where electrons are injected to the plasma with a power-law distribution with the index fixed at $\Gamma_{inj} = 2.5$. The fraction of non-thermal power transferred to the electrons (as opposed to thermal heating) is $\ell_{nth}/\ell_h = 0.84^{+0.03}_{-0.10}$. The best-fitting hard-to-soft compactness ratio is $\ell_h/\ell_s = 0.38^{+0.24}_{-0.15}$ and the optical depth is $\tau = 1.2^{+0.6}_{-0.4}$. The self-consistently computed temperature of the electrons is 11 keV. The disc temperature is $kT_s = 0.54^{+0.02}_{-0.03}$ keV. We also found Compton reflection with the amplitude of $\Omega/2\pi = 0.22^{+0.04}_{-0.12}$ and the reflector ionization of $\lg(\xi/1 \text{ erg cm s}^{-1}) = 4.7^{+0.3}_{-0.8}$. This kind of a spectrum is typical of black hole binaries (e.g. Gierliński et al. 1999; Frontera et al. 2001) in the soft state.

Contrary to the hard state (Section 4.1), the rms spectrum is very well described by the two-component model, where disc and Comptonization are allowed to vary in normalization only. We show this model, with dominant variability of Comptonization, in Fig. 2(a), with the dashed (red in colour) curve. A characteristic feature of this model is a break at around 7 keV, above which Comptonization dominates the spectrum (see Fig. 2b) and rms(E) becomes flat. The energy of this break is directly related to the disc temperature and we found that rms(E) saturates at $\sim 15 kT_s$.

Another model that can explain rms increasing with energy is variable hard power input (Z02). This is opposite to the soft photon input variability in the hard state: this time we kept ℓ_s constant and allowed ℓ_h to vary. This caused the energy spectrum to vary in a way depicted in Section 5 (see Fig. 4(b) below). The result for $r(\ell_h) = 17\%$ is shown by the dotted (cyan in colour) curve in Fig. 2(a). The rms(E) pattern predicted by this model matches the data well, except for the deficiency in rms below ~ 4 keV. We have accounted for this deficiency by adding little variability in the disc. The total rms spectrum (solid curve) matches the data well, and is similar in shape to the two-component model. The energy of the break at ~ 10 keV is also directly related to the seed photon temperature. As in the hard state, the lognormal distribution of ℓ_h produced very similar results to the Gaussian distribution.

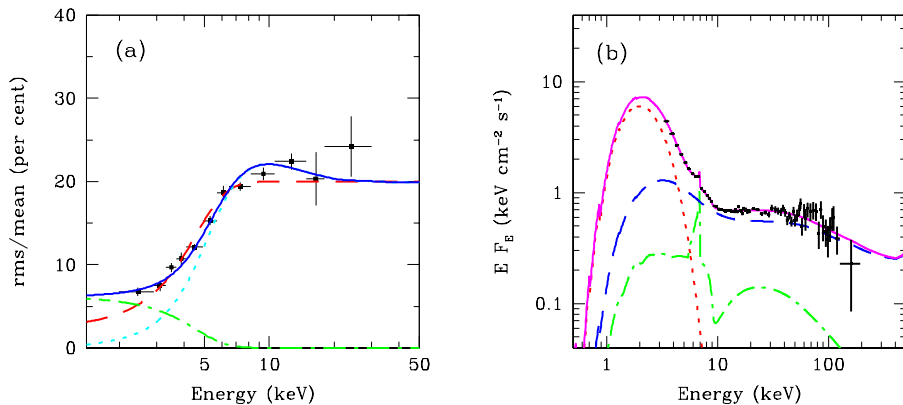


Figure 2. (a) Soft state (obsid 60113-01-18-01) rms spectrum of XTE J1650–500. The dashed curve (red in colour) represents the two-component variability model, with $r(N_s) = 0\%$ and $r(N_h) = 20\%$. The solid curve (blue in colour) shows the model with varying hard compactness (dotted curve, cyan in colour) at $r(\ell_h) = 17\%$ plus additional soft component normalization variability (dash-dotted curve, green in colour) with $r(N_s) = 7\%$. (b) The energy spectrum of the same observation. The model components are identical to those in Fig. 1(b), except for Comptonization taking place in the hybrid, thermal/non-thermal plasma.

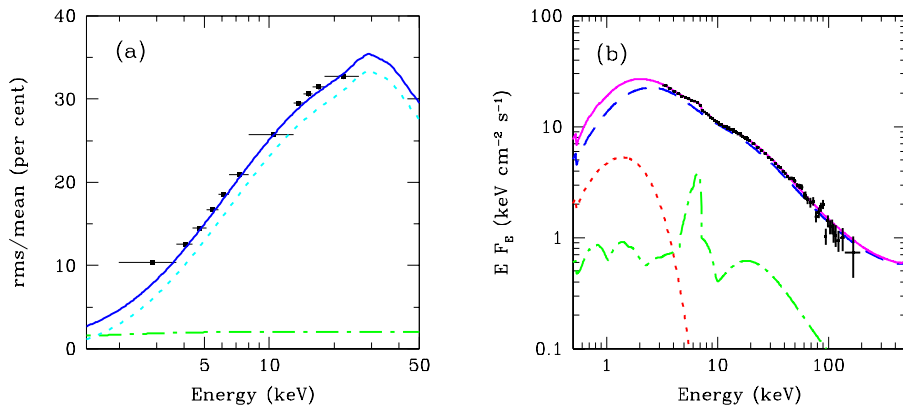


Figure 3. (a) Very high state (obsid 30191-01-01-00) rms spectrum of XTE J1550–564. The solid curve (blue in colour) represents the model of variability consisting of varying hard compactness (dotted curve, cyan in colour) with $r(\ell_h) = 17\%$ plus additional hard component normalization variability (dash-dotted curve, green in colour) with $r(N_h) = 2\%$. (b) The energy spectrum of the same observations. The model components are identical to those in Fig. 1(b), except for Comptonization taking place in the hybrid, thermal/non-thermal plasma.

4.3 Very high state

Fig. 3(a) shows rms spectrum of another black hole XTE J1550–564 in the very high spectral state. Like in the soft-state spectrum in Fig. 2(a), the fractional variability increases with energy, though there is neither break nor saturation up to at least ~ 20 keV.

The very high state energy spectrum of XTE J1550–564 (Fig. 3b) is well described by hybrid Comptonization (see also Gierliński & Done 2003) with weak apparent contribution from unscattered disc photons. The best-fitting model ($\chi^2_\nu = 117/122$) parameters are: hard-to-soft compactness ratio, $\ell_h/\ell_s = 0.80^{+0.08}_{-0.03}$, non-thermal fraction, $\ell_{\text{nth}}/\ell_h = 0.83^{+0.06}_{-0.15}$, electron injection power-law index of $\Gamma_{\text{inj}} = 3.3^{+0.1}_{-0.2}$, and the optical depth of $\tau = 4.73^{+0.35}_{-0.10}$. The electron temperature is 4 keV, and the disc temperature is $kT_s = 0.52^{+0.06}_{-0.09}$ keV. The reflection amplitude is $\Omega/2\pi = 0.20^{+0.16}_{-0.11}$ and its ionization, $\lg(\xi/1 \text{ erg cm s}^{-1}) = 3.6^{+0.2}_{-1.1}$.

The two-component variability that has successfully described the soft-state rms spectrum cannot explain the very high state data, as it predicts a break at ~ 6 keV and flat rms(E) above the break

(similar to the model shown in Fig. 2a). The flattening of rms(E) occurs always at energies where Comptonization dominates and does not depend on its spectral shape. On the other hand, the ℓ_h variability model matched the data very well, though some additional hard component variability contribution was required, similarly to the hard state. Interestingly, in the soft state, the ℓ_h variability created rms(E) pattern with a break at $\sim 15kT_s$, which is not seen here until about 30 keV. And again, using the lognormal distribution of ℓ_h had very little effect on our results.

5 PATTERNS OF VARIABILITY

In previous section, we have presented characteristic rms spectra in three X-ray spectral states and possible models matching these spectra. Certainly, the two-component model where the disc and Comptonization vary independently is only a zeroth-order approximation. Except for a specific case described in Section 6 below, there should be a feedback: a change in the disc luminosity changes the supply of the seed photons for Comptonization, which in turn

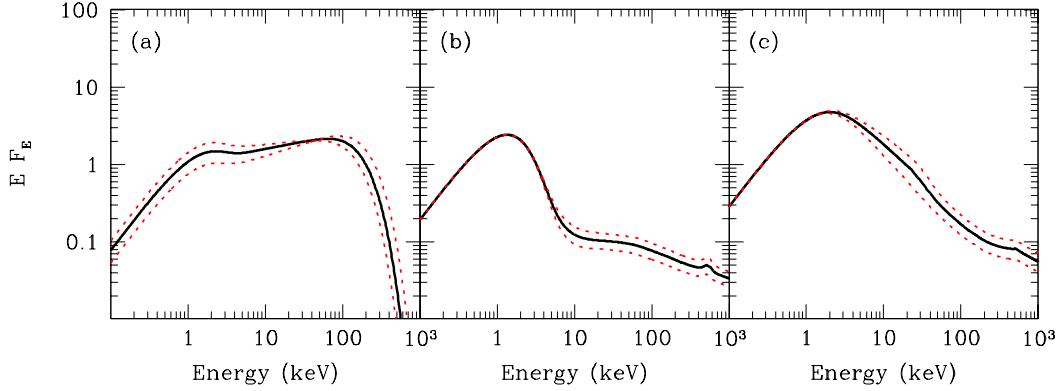


Figure 4. Visualization of model spectral variability (dotted curves, red in colour) with respect to the best-fitting spectrum in a given state (solid black curve). (a) Hard state: variability of the soft photon input, ℓ_s . (b) Soft state and (c) very high state: variability of the hard power, ℓ_h .

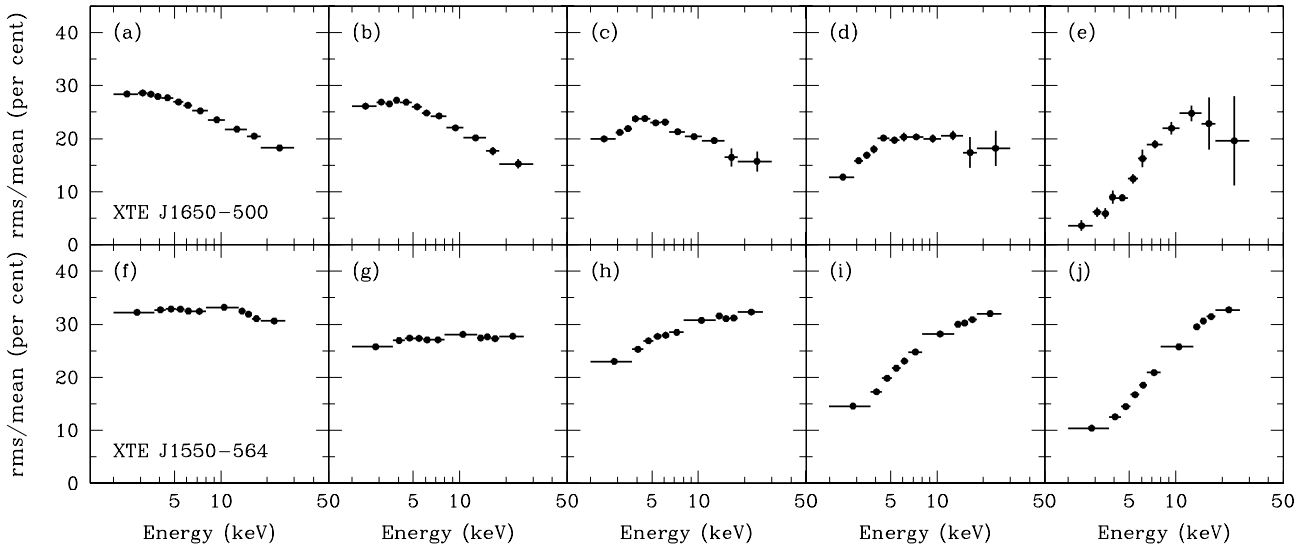


Figure 5. Characteristic patterns of $\text{rms}(E)$ variability observed from two Galactic black hole binaries. The upper row shows the evolution XTE J1650–500 during its outburst and transition from the hard (a) through the intermediate (b–c) to the soft (d–e) spectral state. Spectra from observations 60113-01-X are shown, where X is: (a) 04-00, (b) 08-00, (c) 12-00, (d) 13-01 and (e) 24-00. The lower row shows the evolution of XTE J1550–564 in the beginning of its 1998 outburst and transition from the hard to the very high state. Spectra from observations 30188-06-X are shown, where X is: (f) 01-00, (g) 01-02, (h) 04-00, (i) 06-00, and (j) is from 30191-01-01-00.

should affect the spectral shape of the Comptonized component. Therefore, the models based on varying a parameter in a physical model where the disc and Comptonization are linked together should provide better physical picture of variability.

In Fig. 4, we visualize model spectral variability in each spectral state, with varying soft photon input and hard compactness. For simplicity, we do not include additional variability components required by the data (see Figs. 1, 2 and 3).

In Fig. 5, we show several characteristic rms spectra from XTE J1650–500 and XTE J1550–564 covering hard, soft and very high spectral states. We also show the corresponding power density spectra in Fig. 6. These PDS were extracted over the same frequency band [(1/512)–128 Hz] as those used for creation of the rms spectra. To illustrate energy dependence we show the low- ($\lesssim 13$ keV) and high-energy ($\gtrsim 13$ keV) power spectra. Clearly, in many cases not only the normalization, but also the PDS shape changes as a function of energy.

Below, we discuss in details possible variability models in each of the spectral states shown in Figs. 5–6 and give their theoretical interpretation.

5.1 Hard state

In the hard state, the rms spectrum is either flat (Fig. 5f,g) or smoothly decreasing with energy (Fig. 5a,b). The flat $\text{rms}(E)$ simply corresponds to a situation where the entire spectrum (or Comptonization only, when the disc is not visible in the observed bandwidth) varies in normalization (luminosity) but not in spectral shape (see also Z02). If we assume that luminosity variations are due to changes in the accretion rate, then the only spectral effect we might expect is weak variation in the shape of the high-energy cut-off $\gtrsim 100$ keV, as the optical depth varies following variations in the flow density. We have considered a particular model of the advection dominated flow, where $\tau \propto L^{2/7}$ (Zdziarski 1998). The result

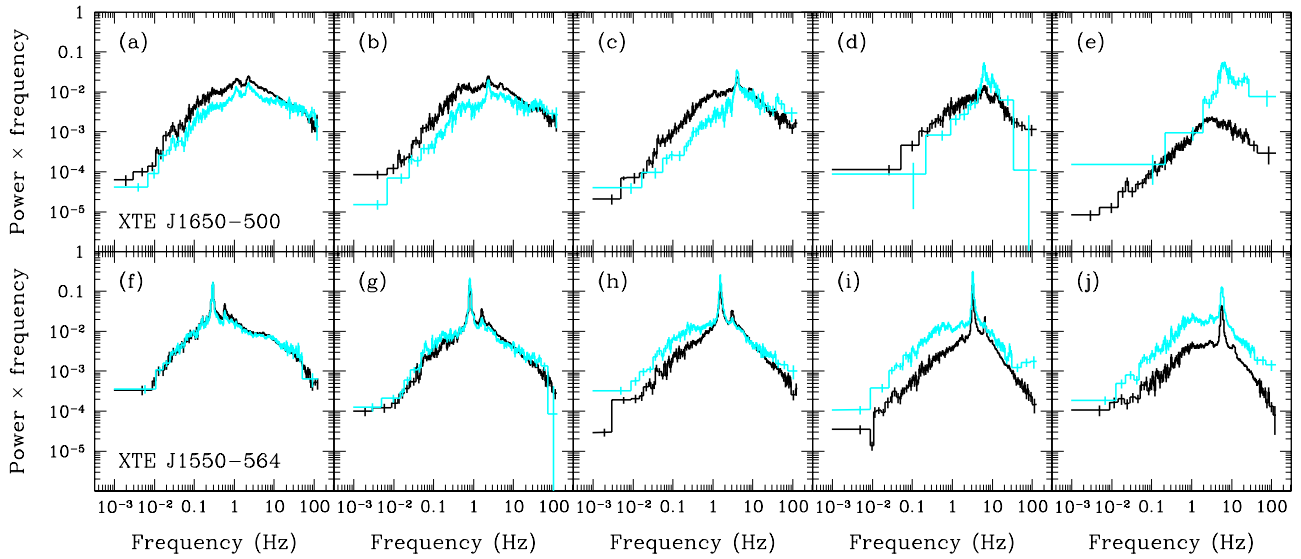


Figure 6. The power density spectra corresponding to the $\text{rms}(E)$ dependencies shown in Fig. 5. The low- and high-energy PDS are shown in black and grey (cyan in colour), respectively. The low-energy band corresponds to the PCA absolute channels 0–25 (XTE J1650–500) and 0–35 (XTE J1550–564). The high-energy band corresponds to the channels above those up to the channel 71. The energies corresponding to these two bands are ~ 2 to ~ 13 and ~ 13 to ~ 25 keV, respectively. The spectra have been rebinned for clarity. Note the maximum of the frequency times power shown here corresponds to the maximum of the variability power per log of frequency.

is shown in Fig. 7(a) with a solid grey (red in colour) curve. The minimum at ~ 300 keV is due to fortuitous intersection of the spectra resulting from this variability prescription at that energy. Additionally, we have checked the result of replacing the thermal Comptonization by that with fully non-thermal injection ($\ell_{\text{nth}}/\ell_{\text{h}} = 1$), which turns out to be negligible at $\lesssim 100$ keV (dotted curve).

The other pattern observed in the hard state is the rms smoothly decreasing with energy. Z02 explained a similar pattern observed on much longer timescales by variable seed photon input, ℓ_{s} . We found this solution consistent with our observations. The result of this model is plotted in Fig. 7(a) with a solid black curve. The characteristic feature of this type of variability is pivoting of the spectrum around ~ 20 – 50 keV (Fig. 4a). Because of that, the $\text{rms}(E)$ reaches a very deep minimum around this energy, so the decline in rms above ~ 5 keV is very steep, and steeper than that observed (see Fig. 1a). This can be understood when we notice that in our model we assumed variations in ℓ_{s} only, with Comptonizing plasma simply responding to these changes in the seed photons, while the data required some variation in the power released in the Comptonized component, ℓ_{h} . The full treatment of this problem within our model would require two-dimensional variation in ℓ_{s} and ℓ_{h} , with some particular relation between the two parameters assumed. For the sake of simplicity, in Section 4.1 we allowed for variations in just one parameter (ℓ_{s}) and added a separate $\text{rms}(E)$ component corresponding to variations in the hard component luminosity. This may correspond to an intermediate case between the flat-rms constant spectral shape model and pure seed photon input variations.

The dotted curves in Fig. 7 show the effect of non-thermal acceleration in the hot plasma. Because it is dominated by the Compton cooling (and often termed as a photon-starved plasma), the electrons in the hard state are efficiently thermalized even when the power provided to them is entirely in the form of non-thermal acceleration (Coppi 1999; Zdziarski, Coppi & Lamb 1990). The effect on the energy spectrum is visible only at high energies and diffi-

cult to measure (McConnell et al. 2002). Our PCA/HEXTE spectrum from Section 4.1 can be fitted by Comptonization with thermal and non-thermal electron injection equally well. The $\text{rms}(E)$ of the thermal spectrum tends to rise steeply at around high-energy cutoff. This is because the spectrum around the cutoff varies in the direction perpendicular to the curve representing the spectrum (Fig. 4a), due to changes in the electron temperature as it adjusts itself to satisfy the energy balance (Z02). However, when a slight non-thermal tail added to the spectrum, the rms does not increase that dramatically and the high-energy variability pattern resembles that one in the soft state (Fig. 4b).

We have also investigated rms spectra resulting from varying seed photon temperature and optical depth of the Comptonizing plasma. The results (Fig. 7b) are highly inconsistent with observations, restricting our models to the variability in ℓ_{s} and luminosity, as discussed above.

An interesting feature of the ℓ_{s} variability in the hard state is its dependence on the seed photon temperature. The rms becomes constant below a certain energy, directly related to the temperature of the seed photons. In our best-fitting model from Section 4.1, the seed photons originate from the soft component of temperature of ~ 0.7 keV, and the $\text{rms}(E)$ flattens below ~ 2 keV (Fig. 4a). We would like to point out that the soft component in this particular model *cannot* be a standard Shakura-Sunyaev disc (Shakura & Sunyaev 1973), as it is too hot (~ 0.7 keV) and too small [$R_{\text{in}} \approx 18$ km for a distance of 4 kpc (Tomsick et al. 2003) and inclination of 30° (Sánchez-Fernández et al. 2002)] for a disc. Instead, we probably see the so-called soft excess, an additional thermal Comptonization component hotter than the disc (see, e.g., Di Salvo et al. 2001; Frontera et al. 2001). The dashed curve in Fig. 7(a) shows an alternative model in which the seed photon temperature was 0.1 keV and the soft excess was fitted as an additional component (which variability was not modelled). Clearly, the slope of $\text{rms}(E)$ below ~ 2 keV is distinctly different from the model in which the seed photons came from the observed soft excess. It is arguable whether

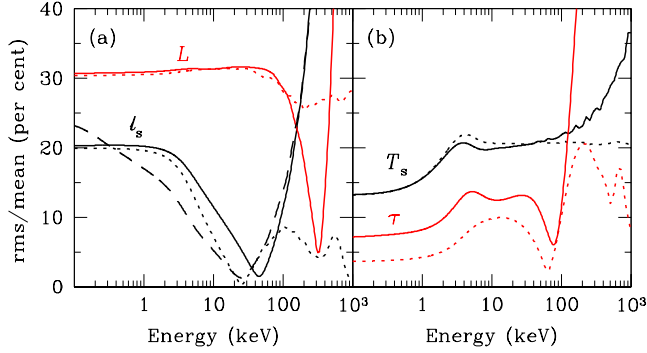


Figure 7. Models of $\text{rms}(E)$ variability in the hard state. (a) Variability of soft photon input, $r(\ell_s) = 20\%$, and of the total luminosity, $r(L) = 30\%$, assuming $\tau \propto L^{2/7}$. (b) Variability of seed photon temperature, $r(T_s) = 5\%$, and of optical depth, $r(\tau) = 50\%$. Solid curves correspond to the best-fitting thermal model from Section 4.1, dotted curves correspond to the same model, but with non-thermal fraction set to 1. The dashed curve in panel (a) represents ℓ_s variability of an alternative (thermal) model with the seed photon temperature set to 0.1 keV.

the flattening of $\text{rms}(E)$ at low energies is present in the hard-state data (Fig. 1a) and additional data from instruments sensitive below 1 keV (e.g., *XMM-Newton* or *Chandra*) are required to confirm its veracity. If flattening is real then the seed photons are not from the disc (or at least not entirely from the disc) but from the soft excess. This can yield crucial constraints on the origin of the soft excess and geometry of the accretion flow.

5.2 Soft state

Soft-state rms spectra are distinctly different from hard state ones. While the hard state typically showed either flat rms or a decrease in power with energy, $\text{rms}(E)$ increases and then saturates at higher energies in the soft state (see also Zdziarski et al. 2005). Similar spectral changes have been also reported in variability of QPOs (e.g. Rodriguez et al. 2004a). The panels (b), (c) and (d) in Fig. 5 show transition from the hard to the soft state. An interesting feature of these spectra is the break at $\sim 2\text{--}4$ keV, present throughout the transition.

Using our best-fitting non-thermal spectral model, we have found in Section 4.2 two similar $\text{rms}(E)$ models that match the observed rms spectrum. The first one assumed variability in the hard component normalization, N_h , only. It produces a quick increase in rms and saturation above a few keV, as shown in Fig. 8(a) with the black curve. The grey (cyan in colour) curves show the effect of different T_s .

The second model involves constant ℓ_s and variable ℓ_h . Unlike the previous model, it takes into account spectral response of Comptonization to the changing ratio of the power released in the corona to that in the disc. On the other hand, changes in the spectral shape of Comptonization (at least in the non-thermal case) are rather small, so the rms spectrum produced by the ℓ_h variability is similar to the one from N_h variability: a quick rise and saturation at higher energies (Fig. 8b).

Our models do not always predict a flat rms above the break energy. In Fig. 8(b), we also show (dashed and dot-dashed curves) the effect of decreasing fraction of the non-thermal acceleration in the total power, ℓ_{nth}/ℓ_h . As the thermal heating becomes more im-

portant, a peak around 20–30 keV in $\text{rms}(E)$ is created. We discuss the origin of this peak in the next section.

A common property of both models is a break in the spectrum followed by flat $\text{rms}(E)$ at higher energies. The formation of the break and flat rms can be seen in the XTE J1650–500 data following its evolution from the intermediate to soft state in Figs. 5(b–d). As mentioned above, the flat $\text{rms}(E)$ is due to a spectral component varying in normalization but not in shape. The break corresponds to an energy in the spectrum above which Comptonization dominates, which is roughly at $15 kT_s$ (the best-fitting seed photons temperature was 0.54 keV).

As in the hard state, variability of either the seed photon temperature, T_s , or the optical depth of the hot plasma, τ , do not provide $\text{rms}(E)$ patterns consistent with the data (Fig. 8a, c).

ZO2 considered variability in the hardness of the power-law electrons injected into the hot plasma. This can be done in two ways, either by varying the injection index, Γ_{inj} , or by varying the high-energy cutoff in the electron distribution represented by the maximum Lorentz factor, γ_{max} . ZO2 concluded that the first pattern was inconsistent with the colour-colour and colour-luminosity correlations, while the last one provided a good fit, though they have not analysed rms spectra emerging from these patterns. Here we calculate the exact form of $\text{rms}(E)$ both for varying Γ_{inj} and γ_{max} . We find that both of them create very similar rms spectra, and we show one of them (Γ_{inj}) in Fig. 8(d). Both patterns are characterized by a strong rms peak around ~ 10 keV and are clearly inconsistent with any rms spectrum found by us so far. Therefore, we conclude that neither Γ_{inj} nor γ_{max} variability can explain the observed $\text{rms}(E)$ patterns.

5.3 Very high state

The very high state energy spectrum is dominated by a strong non-thermal Comptonized tail (Fig. 3b; see also Gierliński & Done 2003). The relative contribution from the disc is much weaker than in the soft state and the Comptonized tail is much softer than in the hard state. The rms spectra are also distinctly different. Panels (f–j) in Fig. 5 show evolution of the rms from the hard to the very high state. The initially flat $\text{rms}(E)$ becomes very steep, increasing with energy without any apparent break up to at least ~ 20 keV.

We have investigated the same patterns of variability as in the soft state, using the best-fitting model from Section 4.3. The results are shown in Fig. 9. The simplest model of N_h variability (or, more general, two-component variability) does not work here. As the entire energy spectrum is dominated by Comptonization, the resulting $\text{rms}(E)$ is almost flat in this model, with a slight depression below ~ 3 keV. The observed strongly increasing $\text{rms}(E)$ requires the Comptonized tail to vary in spectral shape, not only in normalization. In Section 4.3, we have found that ℓ_h variability matches the data well. Fig. 9(b) now shows the dependence of ℓ_h variability models on the seed photon temperature and non-thermal fraction.

A common feature of ℓ_h variability patterns in the soft and very high states is formation of a peak in the rms spectrum at about 20–30 keV when thermal heating is present in the Comptonizing plasma, i.e., when ℓ_{nth}/ℓ_h is less than 1. The origin of the peak can be understood from the decomposition of the hybrid Comptonization spectrum into thermal and non-thermal components (following the method of Hannikainen et al. 2005). This decomposition is shown in Fig. 10(a) for the very high state spectrum where the non-thermal fraction was set to $\ell_{\text{nth}}/\ell_h = 0.4$, corresponding to $\text{rms}(E)$ shown in Fig. 10(b). The peak in $\text{rms}(E)$ is due to variations in the high-energy cutoff of the thermal component. A similar kind

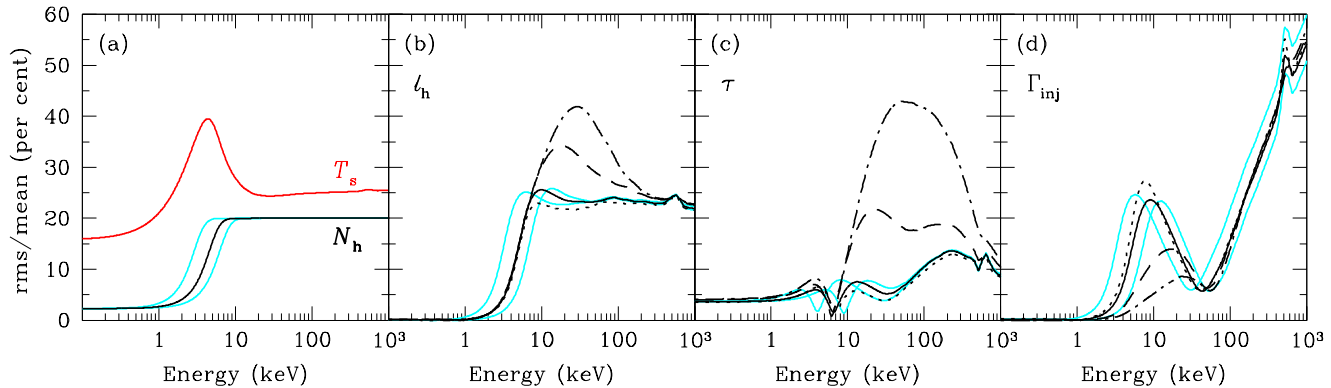


Figure 8. Models of rms(E) variability in the soft state. (a) Variability of the hard component normalization, $r(N_h) = 20\%$ and of the seed photon temperature, $r(T_s) = 6\%$. (b) Variability of the hard compactness, $r(\ell_h) = 20\%$, (c) the optical depth, $r(\tau) = 50\%$, and (d) the electron injection index, $r(\Gamma_{inj}) = 20\%$. Solid curves correspond to the best-fitting hybrid model from Section 4.2. Grey (cyan in colour) curves on each side of the solid curve show the same model, but with seed photon temperature altered by ± 0.2 keV with respect to the best fit. Dotted, dashed and dot-dashed black curves correspond to $\ell_{nth}/\ell_h = 1.0, 0.4$ and 0.2 , respectively.

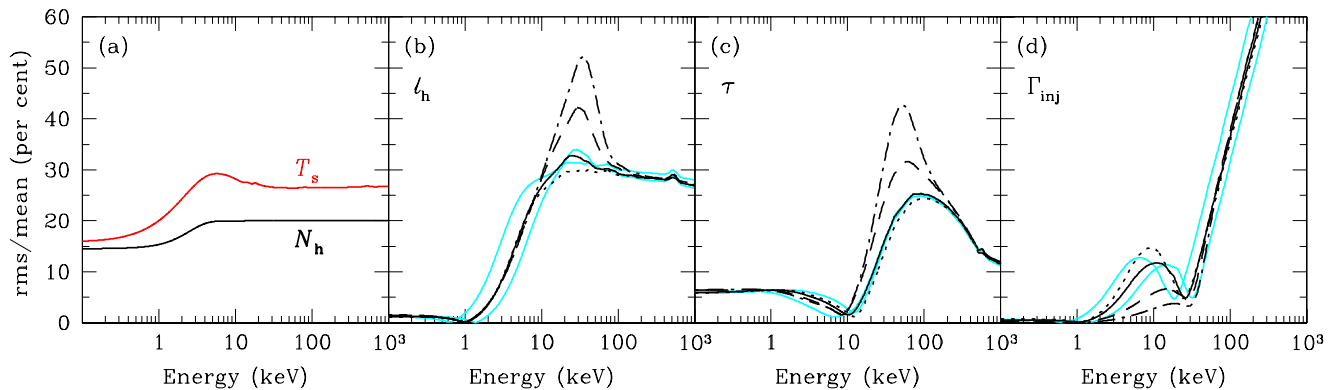


Figure 9. Models of rms(E) variability in the very high state. (a) Variability of the hard component normalization, $r(N_h) = 20\%$, and of the seed photon temperature, $r(T_s) = 6\%$. (b) Variability of the hard power, $r(\ell_h) = 20\%$, (c) the optical depth, $r(\tau) = 20\%$, and (d) the electron injection index, $r(\Gamma_{inj}) = 20\%$. Solid curves correspond to the best-fitting hybrid model from Section 4.3. Grey (cyan in colour) curves on each side of the solid curve show the same model, but with seed photon temperature altered by ± 0.2 keV with respect to the best fit. Dotted, dashed and dot-dashed black curves correspond to $\ell_{nth}/\ell_h = 1.0, 0.4$ and 0.2 , respectively.

of variability can be seen in the hard state (Fig. 4a) and it causes a dramatic increase in the rms(E), as seen in Fig. 7(a). In the case of the very high state, though, the increase is suppressed at higher energies, where the non-thermal component begins to dominate. With increasing contribution of thermal heating, the peak becomes stronger. This is an important feature of hybrid Comptonization and it will be interesting to see whether it is detected in future observations.

The very high state rms spectrum of XTE J1550–564 shown in Fig. 3(a) rises with energy until about 25 keV, i.e. until the last PCA energy channel we use in this paper. In Fig. 11, we show the same spectrum computed up to energy of 67 keV. The last two data points (filled boxes) correspond to the rebinned absolute PCA data channels 72–89 and 90–174. There is a clear increasing trend in the rms, not consistent with the ℓ_h variability model. However, one should treat the PCA data above ~ 30 keV, where background contribution becomes important, with great caution. To test the accuracy of background estimate we have looked into our PCA/HEXTE energy spectrum with its best-fitting model from Section 4.3. We extended the PCA energy spectrum up to about 67 keV and compared addi-

tional energy channels with the best-fitting model to our standard PCA/HEXTE spectrum. It occurred that the PCA flux in additional high-energy channels was significantly lower than in the model, most likely due to the overestimated PCA background. The model-to-data ratio in the energy bins corresponding to the two additional points in Fig. 11 was 0.93 and 0.82. We have introduced these corrections to the mean count rate in computed fractional rms (which is rms/mean). The corrected data points are shown in Fig. 11 by open triangles. Now they appear to be consistent with the ℓ_h variability model. We would like to stress that by doing this we have pushed the PCA data to the limits where systematic uncertainties are not very well known. Therefore this result should be treated with caution.

Finally, we have calculated model variability patterns for varying T_s , τ and Γ_{inj} (Fig. 9a, c, d). As it was the case in the soft state, we found them not consistent with the data.

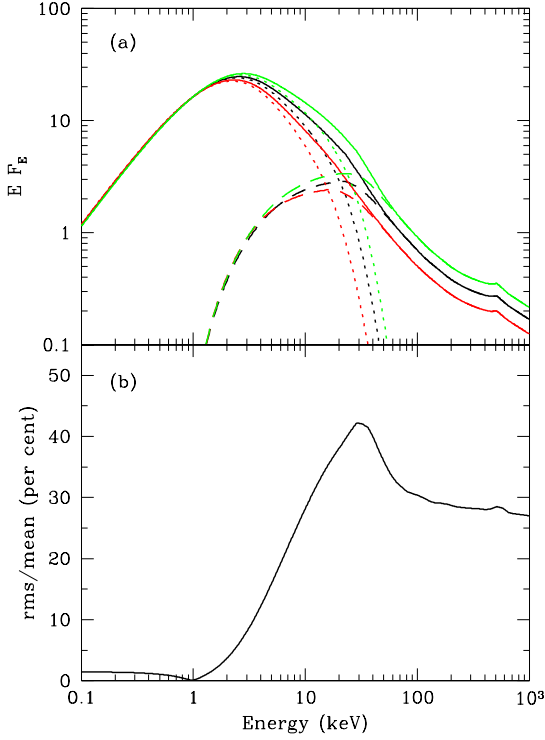


Figure 10. (a) Visualization of model spectral variability in the very high state due to changes of ℓ_h . The model shown corresponds to the non-thermal fraction $\ell_{\text{nth}}/\ell_h = 0.4$. The three spectra correspond to variation in ℓ_h by ± 20 per cent (top and bottom) and the original spectrum (middle). The dotted and dashed curves represent thermal and non-thermal components of the hybrid Comptonization. (b) The corresponding rms spectrum. The peak at ~ 30 keV is due to the variability of the high-energy cutoff of the thermal-Compton component.

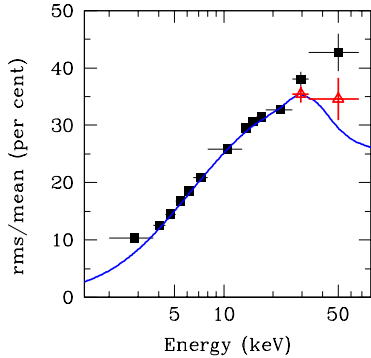


Figure 11. The rms spectrum and model of the very high state from Section 4.3 (see Fig. 3a). Here, we have extended the energy scale to the limits of PCA capabilities. The squares show the direct extension of the spectrum, calculated in the standard way, as described in Section 2, which is clearly incompatible with our best model. The triangles show the rms corrected for the background excess, estimated from the broad-band PCA/HEXTE energy spectrum.

6 ACCRETION FLOW GEOMETRY

Z02 considered a truncated disc geometry to explain the observed $\text{rms}(E)$ patterns. Within this model, in the hard state the accretion disc is truncated at some radius and replaced by a hot optically thin inner flow (e.g. Poutanen, Krolik & Ryde 1997; Esin, McClintock & Narayan 1997). Variations in the inner disc radius provide the necessary change in the soft photon input that can explain the observed $\text{rms}(E)$. However, Z02 analysed the long-term variability of Cyg X-1 on timescales of days and months, much longer than the viscous timescale, so significant variations in the inner disc radius are possible. This is not the case on the timescales of milliseconds and seconds, observed here. The radial drift velocity in the accretion disc at 0.05 of the Eddington luminosity truncated at $20GM/c^2$ around a $10M_\odot$ black hole is $\sim 4 \text{ km s}^{-1}$ in the radiation pressure dominated zone (Shakura & Sunyaev 1973). The timescale required to change the truncation radius by e.g. $10GM/c^2$ is ~ 20 s. When the disc is truncated farther away, this timescale is even longer. Clearly, there must be another mechanism for varying soft photon input.

Most of the rapid X-ray variability models assume some kind of oscillations in the accretion flow. It is not yet clear how these oscillations can be converted into the observed modulation of X-ray flux. Our result suggests that in the hard state this happens via modulation of the seed photons for Comptonization. In the model of Giannios & Spruit (2004), oscillations in the hot inner flow are excited by variations in the Compton cooling rate. During oscillations, the inner flow changes its Compton y parameter, which results in the pivoting of the Comptonized spectrum. This is in agreement with observations and our $\text{rms}(E)$ models. The drifting-blob model of Böttcher & Liang (1999), where the local seed photon input varies as the blob travels through inhomogeneous hot flow, predicts increase of the rms with energy, contrary to what is observed.

According to the truncated disc model in the soft (and probably very high) state, the cold disc extends down to the marginally stable orbit and the Comptonized emission originates from the active regions or corona above the disc (e.g. Gierliński et al. 1999; Poutanen & Fabian 1999). The $\text{rms}(E)$ patterns quickly increasing with energy are consistent with the stable disc and variable corona (see also Churazov, Gilfanov & Revnivtsev 2001). Coronal flares produce most of the power at higher energies (Böttcher, Jackson & Liang 2003), so naturally we expect most variability at photon energies $\gtrsim 10$ keV.

The two $\text{rms}(E)$ models we considered in Section 4.2 can be explained within the disc-corona geometry. The model with varying Comptonized normalization (but not spectral shape) can correspond to a scenario in which the covering fraction of the (patchy) corona varies, due to e.g. new flares being formed, and the ℓ_h/ℓ_s ratio for each flare is roughly the same, so the spectral shape of Comptonization does not vary. However, with changing number of flares (covering fraction), the luminosity of Comptonization would change, hence the observed high-energy variability. Since the uncovered fraction of the disc changes as well, we should expect some variability in the disc. The very small disc variability found in this model (Fig. 2a) requires a small covering fraction of the corona, $\lesssim 10$ per cent.

The model with varying ℓ_h may correspond to changing power in the corona without changing the covering fraction. In the soft state of XTE J1650–500, it required $r(\ell_h) \approx 17\%$ and additional 7% variability in the disc (Fig. 2a). A quick estimate shows that this is the level of variability is expected from reprocessing of hard Comptonized photons in the disc. In the energy spectrum shown in

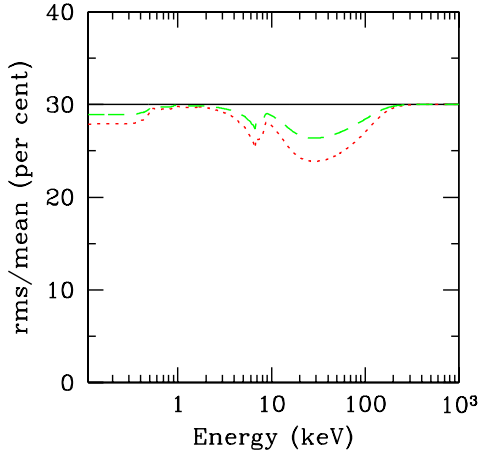


Figure 12. The effect of Compton reflection on $\text{rms}(E)$ variability. The energy spectrum used for this simulation is the best-fitting model to the hard state. The curves represent a simple two-component model, where the continuum and reflection vary in normalization only but not in spectral shape. Solid curve: continuum and reflection are correlated, and vary with the same relative amplitude of 30%. Dotted curve: both components are uncorrelated, and vary with the same amplitude. Dashed curve: both components are correlated, but the reflection variability amplitude is 15%, i.e., a half of the continuum amplitude.

Fig. 2(b), the Comptonized component luminosity, L_h , is roughly 0.4 of the disc luminosity, L_s . If we consider a corona or active regions above the disc, then we would expect less than a half of L_h to be absorbed and re-emitted by the disc, which constitutes $\lesssim 0.2$ of L_s . Since the coronal variability is about 20%, the expected variability of the disc from reprocessing is $\lesssim 4\%$, in a rough agreement with the observed rms of 7%. The remaining fraction of variability might be intrinsic to the disc.

7 REFLECTION

We have neglected the effects of Compton reflection in our variability models so far. Here, we perform a simple test of possible effects reflection variability can have on the rms spectra. To do this, we take our best-fitting model to the hard state from Section 4.1 as a template. This time, we take into account Compton reflection. We also assume the simplest possible two-component variability model, where the continuum (with the soft and hard components added) and the reflection vary only in normalization, but not in spectral shape. When the continuum and reflection variabilities are correlated (i.e. the covariance $\sigma_{cr} = \sigma_c \sigma_r$) and vary with the same relative amplitude, the resulting $\text{rms}(E)$ is obviously energy-independent (solid curve in Fig. 12). However, strong reflection-related features appear in the rms spectrum (dotted curve in Fig. 12), when continuum and reflection are uncorrelated ($\sigma_{cr} = 0$). Similar features can be seen when they are correlated, but vary with different relative amplitudes (30% and 15% for the continuum and reflection, respectively; dashed curve in Fig. 12). Certainly, this is a very simplified model, but similar features in $\text{rms}(E)$ are generated in our parameter-variability models in all spectral states when we allow for the reflection variability to be detached from the continuum variability, i.e. either uncorrelated, of different amplitude, or entirely independent.

We do not see any obvious such features in the observed rms

spectra (Fig. 5) in any of the spectral states. This provides with an important constraint on the relation between the irradiating X-ray continuum and Compton reflection. As they are well correlated, the reflected component must originate from Compton reprocessing of the *observed* continuum. This also means that the reflection variability (at the frequencies dominating the power spectra used to the analysis, see Fig. 6) is due to variability in the irradiating X-ray continuum and not due to changes in the properties of the reflector (e.g. waves or warps in the disc).

We have pointed out in Section 1 that the $\text{rms}(E)$ spectra presented here have been integrated over a rather wide frequency range, (1/512)–128 Hz, whereas spectral dependence on frequency is possible. It has been known that the amplitude of Compton reflection can strongly decrease at high frequencies, $\gtrsim 10$ Hz, e.g., in the hard state of Cyg X-1 (Revnitsev et al. 1999b; Gilfanov, Churazov & Revnitsev 1999). However, those frequencies contribute relatively little to the integrated PDS used by us (Fig. 6). On the other hand, we note that reflection amplitude changing with frequency would still produce featureless $\text{rms}(E)$ spectrum as long as the *fractional* variability of the reflection remains roughly constant with changing frequency.

8 CONCLUSIONS

We have explained various patterns of the observed energy-dependent X-ray variability in black hole binaries with a model in which the energy spectrum varies in response to a changing physical parameter. Our spectral model consisted of the disc emission and its hybrid (thermal/non-thermal) Comptonization. In the hard state, we found the decreasing $\text{rms}(E)$ consistent with variations in the seed photon input (together with some variation in ℓ_h). In the soft and very high states, the data were consistent with varying power released in the hot Comptonizing plasma. Another model of the soft state involved varying coronal luminosity, without changing spectral shape.

Our models predict a few important features of the $\text{rms}(E)$ spectra. The break in the $\text{rms}(E)$ observed in the soft (and perhaps hard) state is directly related to the seed photon temperature. We estimate it to occur at $\sim 15kT_s$. Thus, rms spectra extending to lower energies than those used in this paper might yield an important constraint on the origin of the soft excess observed in the hard state. In the very high state (and perhaps sometimes in the soft state), our models predict a strong peak in $\text{rms}(E)$ at ~ 30 keV, related to the temperature of the thermal electrons in the hybrid plasma. If this peak is confirmed with high-energy data, it would strongly support the presence of hybrid electrons in the hot plasma. We stress that the presence of the peak requires *hybrid*, not just power-law electrons.

Lack of clear reflection features in the rms spectra implies that the reflection and the X-ray continuum are well correlated and vary with the same amplitude. Therefore, the reflected component originates from the reflection of the observed continuum indeed, and its rapid variability is due to changes in the irradiating continuum, and not due to changes in the reflector properties. We stress, however, that this result applies to the range of frequencies dominating the PCA power spectra of the studied objects, i.e., $\lesssim 10$ Hz.

Z02 studied energy-dependent patterns of variability from Cyg X-1, based on *RXTE/ASM* and *CGRO/BATSE* light curves on timescales from days to months. In this work, we have extended this study to other black hole candidates and to much shorter timescales, from milliseconds to hundreds of seconds. The observed depen-

dence of fractional rms variability on energy is very similar in both cases, despite very different timescales. Moreover, similar patterns have been observed from PDS components, like QPOs (e.g. Rodriguez et al. 2004a, b; Zdziarski et al. 2005), also in the case of neutron-star binaries (e.g. Gilfanov et al. 2003). Clearly, there is a common physical mechanism behind those rms(E) patterns. Their universality indicates their fundamental nature and importance for understanding physics of accretion.

On the other hand, significant difference in timescales *implies* different physics. While Z02 explained hard-state variability by changing inner disc radius, it cannot operate on timescales of milliseconds, which are much shorter than the viscous timescale. In both cases the common underlying mechanism is modulation of hard X-rays by the varying seed photon input, however the dynamical link between the cold disc and hot Comptonizing region must be different.

ACKNOWLEDGEMENTS

We thank Chris Done for stimulating discussions and the referee, Juri Poutanen, for valuable suggestions. This paper was supported through KBN grants 1P03D01827, 1P03D01727, PBZ-KBN-054/P03/2001 and 4T12E04727. MG acknowledges support through a PPARC PDRF.

REFERENCES

- Berger M., van der Klis M., 1994, *A&A*, 292, 175
 Böttcher M., Liang E. P., 1998, *ApJ*, 506, 281
 Böttcher M., Liang E. P., 1999, *ApJ*, 511, L37
 Böttcher M., Jackson D. R., Liang E. P., 2003, *ApJ*, 586, 389
 Bursa M., Abramowicz M. A., Karas V., Kluźniak W., 2004, *ApJ*, 617, L45
 Churazov E., Gilfanov M., Revnivtsev M., 2001, *MNRAS*, 321, 759
 Coppi P. S., 1999, in Poutanen J., Svensson R., eds, *ASP Conf. Ser. Vol. 161, High Energy Processes in Accreting Black Holes*. ASP, San Francisco, p. 375
 Cui W., Zhang S. N., Chen W., 1998, *ApJ*, 492, L53
 Di Salvo T., Done C., Życki P. T., Burderi L., Robba N. R., 2001, *ApJ*, 547, 1024
 Done C., Gierliński M., 2003, *MNRAS*, 342, 1041
 Esin A. A., McClintock J. E., Narayan R., 1997, *ApJ*, 489, 865
 Frontera F., et al., 2001, *ApJ*, 546, 1027
 Giannios D., Spruit H. C., 2004, *A&A*, 427, 251
 Gierliński M., & Done C. 2003, *MNRAS*, 342, 1083
 Gierliński M., Zdziarski A. A., Done C., Johnson W. N., Ebisawa K., Ueda Y., Haardt F., Philips B. F., 1997, *MNRAS*, 288, 958
 Gierliński M., Zdziarski A. A., Poutanen J., Coppi P. S., Ebisawa K., Johnson W. N., 1999, *MNRAS*, 309, 496
 Gilfanov M., Churazov E., Revnivtsev M., 1999, *A&A*, 352, 182
 Gilfanov M., Revnivtsev M., Molkov S., 2003, *A&A*, 410, 217
 Hannikainen D. C., et al., 2005, *A&A*, 435, 995
 Kotov O., Churazov E., Gilfanov M., 2001, *MNRAS*, 327, 799
 Lin D., Smith I. A., Böttcher M., Liang E. P., 2000, *ApJ*, 531, 963
 Magdziarz P., Zdziarski A. A., 1995, *MNRAS*, 273, 837
 McConnell M. L., et al., 2002, *ApJ*, 572, 984
 Mitsuda K., et al., 1984, *PASJ*, 36, 741
 Poutanen J., 2001, *AdSpR*, 28, 267
 Poutanen J., Krolik J. H., Ryde F., 1997, *MNRAS*, 292, L21
 Poutanen J., Fabian A. C., 1999, *MNRAS*, 306, L31
 Psaltis D., Norman C., 2000, *astro-ph/0001391*
 Rao A. R., Naik S., Vadawale S. V., Chakrabarti S. K., 2000, *A&A*, 360, L25
 Revnivtsev M., Borozdin K., Emelyanov A., 1999a, *A&A*, 344, L25
 Revnivtsev M., Gilfanov M., Churazov E., 1999b, *A&A*, 347, L23
 Revnivtsev M., Gilfanov M., Churazov E., 2000, *A&A*, 363, 1013
 Revnivtsev M., Gilfanov M., Churazov E., 2001, *A&A*, 380, 520
 Rodriguez J., Corbel S., Kalemci E., Tomsick J. A., Tagger M., 2004a, *ApJ*, 612, 1018
 Rodriguez J., Corbel S., Hannikainen D. C., Belloni T., Paizis A., Vilhu O., 2004b, *ApJ*, 615, 416
 Sánchez-Fernández C., Zurita C., Casares J., Castro-Tirado A. J., Bond I., Brandt S., Lund N., 2002, *IAUC*, 7989, 1
 Shakura N. I., Sunyaev R. A., 1973, *A&A*, 24, 337
 Titarchuk L., Osherovich V., Kuznetsov S., 1999, *ApJ*, 525, L129
 Tomsick J. A., Kalemci E., Corbel S., Kaaret P., 2003, *ApJ*, 592, 1100
 Uttley P., McHardy I. M., Vaughan S., 2005, *MNRAS*, 359, 345
 van der Klis M., 2004, *AdSpR*, 34, 2646
 Vaughan B. A., Nowak M. A., 1997, *ApJ*, 474, L43
 Vaughan S., Fabian A. C., 2004, *MNRAS*, 348, 1415
 Wardziński G., Zdziarski A. A., Gierliński M., Grove J. E., Jahoda K., Johnson W. N., 2002, *MNRAS*, 337, 829
 Zdziarski A. A., 1998, *MNRAS*, 296, L51
 Zdziarski A. A., 2005, *MNRAS*, 360, 816
 Zdziarski A. A., Gierliński M., 2004, *Progr. Theor. Phys. Suppl.*, 155, 99
 Zdziarski A. A., Coppi P. S., Lamb D. Q., 1990, *ApJ*, 357, 149
 Zdziarski A. A., Poutanen J., Mikołajewska J., Gierliński M., Ebisawa K., Johnson W. N., 1998, *MNRAS*, 301, 435
 Zdziarski A. A., Poutanen J., Paciesas W. S., Wen L., 2002, *ApJ*, 578, 357 (Z02)
 Zdziarski A. A., Lubiński P., Gilfanov M., Revnivtsev M., 2003, *MNRAS*, 342, 355
 Zdziarski A. A., Gierliński M., Rao A. R., Vadawale S. V., Mikołajewska J., 2005, *MNRAS*, 360, 825
 Życki P. T., 2003, *MNRAS*, 340, 639